Available online at www.sciencedirect.com
SCIENCE DIRECT®
Earth and Planetary Science Letters 235 (2005) 141–150
EPSL
www.elsevier.com/locate/epsl

Chronological constraints on processes leading to large active landslides

F. Bigot-Cormier[a,b,*], R. Braucher[a], D. Bourlès[a], Y. Guglielmi[b], M. Dubar[c], J.-F. Stéphan[b]

[a]CEREGE, Plateau de l'Arbois, BP 80, 13545 Aix-en-Provence Cedex 04, France
[b]Géosciences Azur, UMR 6526-CNRS/UNSA, Parc Valrose, 06108 Nice Cedex 02, France
[c]CNRS/CRA, UNSA, 250 rue A. Einstein, 06560 Valbonne-Sophia Antipolis, France

Received 2 November 2004; received in revised form 7 March 2005; accepted 9 March 2005
Available online 26 May 2005
Editor: V. Courtillot

Abstract

Cosmic ray exposure dating of gravitational scarps along a slope nesting a presently active landslide (La Clapière landslide, Tinée valley, Argentera massif, SE France) reveal successive periods of gravitational destabilization. An initial gravitational destabilization at 10.3 ± 0.5 ^{10}Be ka occurs more than 3000 yr after the end of the last deglaciation of the Tinée valley, dated in the studied area from "stoss-and-lee" topography sampled along the Tinée and its tributary Rabuons valleys. A second gravitational destabilization is well constrained at 7.1 ± 0.5 ^{10}Be ka through the dating of two gravitational scarps. Although coincidental with the so-called "climatic optimum", other local or regional triggering factors may be invoked. A third evidenced gravitational destabilization occurred 2.3 ± 0.5 ^{10}Be ka ago. This study thus demonstrates that in situ produced cosmogenic ^{10}Be allows establishing the chronology of gravitational destabilization leading to present major active landslides. However, in the present case, deciphering between the various possible triggering factors will necessitate similar studies on other landslides inside the alpine arc.

Keywords: cosmic ray exposure dating; chronology; landslide; "stoss-and-lee" feature

1. Introduction and geological setting

In Alpine areas, slope decompression following the last deglaciation and subsequent climatic changes have been mainly invoked as causative factors of slope instability that may lead to large-scale landslides [1–4]. Large landslides that recently

* Corresponding author. Géosciences Azur, UMR 6526-CNRS/UNSA, Parc Valrose, 06108 Nice Cedex 02, France.
E-mail addresses: bigot@unice.fr (F. Bigot-Cormier), braucher@cerege.fr (R. Braucher), bourles@cerege.fr (D. Bourlès), guglielmi@geoazur.unice.fr (Y. Guglielmi), dubar@cepam.cnrs.fr (M. Dubar), stephan@geoazur.unice.fr (J.-F. Stéphan).

0012-821X/$ - see front matter © 2005 Elsevier B.V. All rights reserved.
doi:10.1016/j.epsl.2005.03.012

(i.e. within the last hundred years) developed are indeed in many cases nested into presently inactive larger structures that evidence former deep-seated gravitational slope movements [5]. In order to assess the successive processes that may lead to presently active major landslide in a glacial valley, an original method combining morphological and structural studies with cosmic ray exposure (CRE) dating of gravitational induced scarps and trenches has been developed and applied to the La Clapière landslide.

The La Clapière landslide is located in the northwestern part of the external crystalline massif of the Argentera (South of the western Alps, France/Italy) (Fig. 1a). The Argentera basement core consists of two main metamorphic Variscan units [6,7] juxtaposed along the N120–140°E trending Valletta–Mollières mylonitic zone [8]. From the fission track thermochronological method on apatites, we know that the two last tectonic pulses appeared at about 6 Ma in the NW part of the massif and at about 3.5 Ma in the bulk of the massif [9,10]. The studied landslide is located on the left bank of the Tinée river (NW of the Argentera massif), in front of Saint-Etienne de Tinée town (Fig. 1b). The Tinée valley is an old main glacial carved valley connected to some high altitude secondary glaciers like the glacier located in the Rabuons valley. The rock slope is made of gneisses and is affected by faults whose directions are: N010–030°E, N090°E, N110–140°E [11] (Fig. 2A). One of the N090°E faults crosses the Rabuons valley up to the base of the present active landslide (Figs. 1b and 2A,B). The slope is covered with forest with a mean 25° dip.

A rock mass movement entirely affects the La Clapière slope between 1100 m and 2200 m elevation. Two zones can however be distinguished: (1) the La Clapière landslide which corresponds to the zone active for roughly one century according to aerial photographs; and (2) the historically "stable" zone showing displacement rates < 1 mm d^{-1} recorded since the 1970s (Fig. 2A and B). The active zone, which has an estimated volume of ~ 60 millions m^3 [12], overlaps the Quaternary alluvial deposits of the Tinée river (Fig. 1b). At the top of the landslide, a 120 m high scarp extends over a width of 800 m up to an elevation of 1600 m. The depth of the failure surface does not exceed 100 m to 200 m [12]. The landslide itself is divided into compartments limited by pre-existing faults. The main central volume is bounded by the main failure surface and moves downward with 45 to 90 mm d^{-1} N010°E and N115°E motions [12]. The displacement rate can reach 160 to 330 mm d^{-1} at the top of the landslide (Fig. 2b). Extensional deformation structures like large tension cracks and several meters high downhill scarps characterize the historically "stable" zone. Indicative of displacements along penetrative preexisting tectonic joints, these structures evidence that gravitational movements also affected the upper part of the slope, i.e. between 1700 m and 2100 m elevation. Hydrological, structural, geomorphologic and seismic analyses being performed and monitored since the 1970s at this site [11,13,14], the La Clapière landslide is a particularly well-suited natural laboratory to study gravitational processes leading to large-scale landslides.

2. Sampling strategy and methodology

CRE dating utilizes the accumulation of rare nuclides produced through nuclear reactions induced by high-energy cosmic radiation. This accumulation indeed only begins when a rock is exposed at the earth's surface (see review [15]). To date the various events that exposed rocks to the earth's surface in the Tinée valley, we use in situ produced ^{10}Be resulting from spallation reactions on Si and O, since all samples coming from the metamorphic basement are gneisses and migmatites.

To obtain information on the chronology of the last deglaciation in the Tinée valley, samples for CRE dating from glacial landforms such as "stoss-and-lee" topography and glacial polished surfaces, whose exposition to cosmic rays begins when the glacier retreats, were collected in the studied area.

To determine the timing of the gravitational deformations affecting the La Clapière slope and the left bank of the Rabuons valley, samples for CRE dating were collected along gravitational bedrock scarps (Fig. 3A).

Note that for one site (site A, Fig. 1b), a glacial polished surface is affected by a scarp. Then for this site, we collected two samples (Tin 03-09, Tin 03-

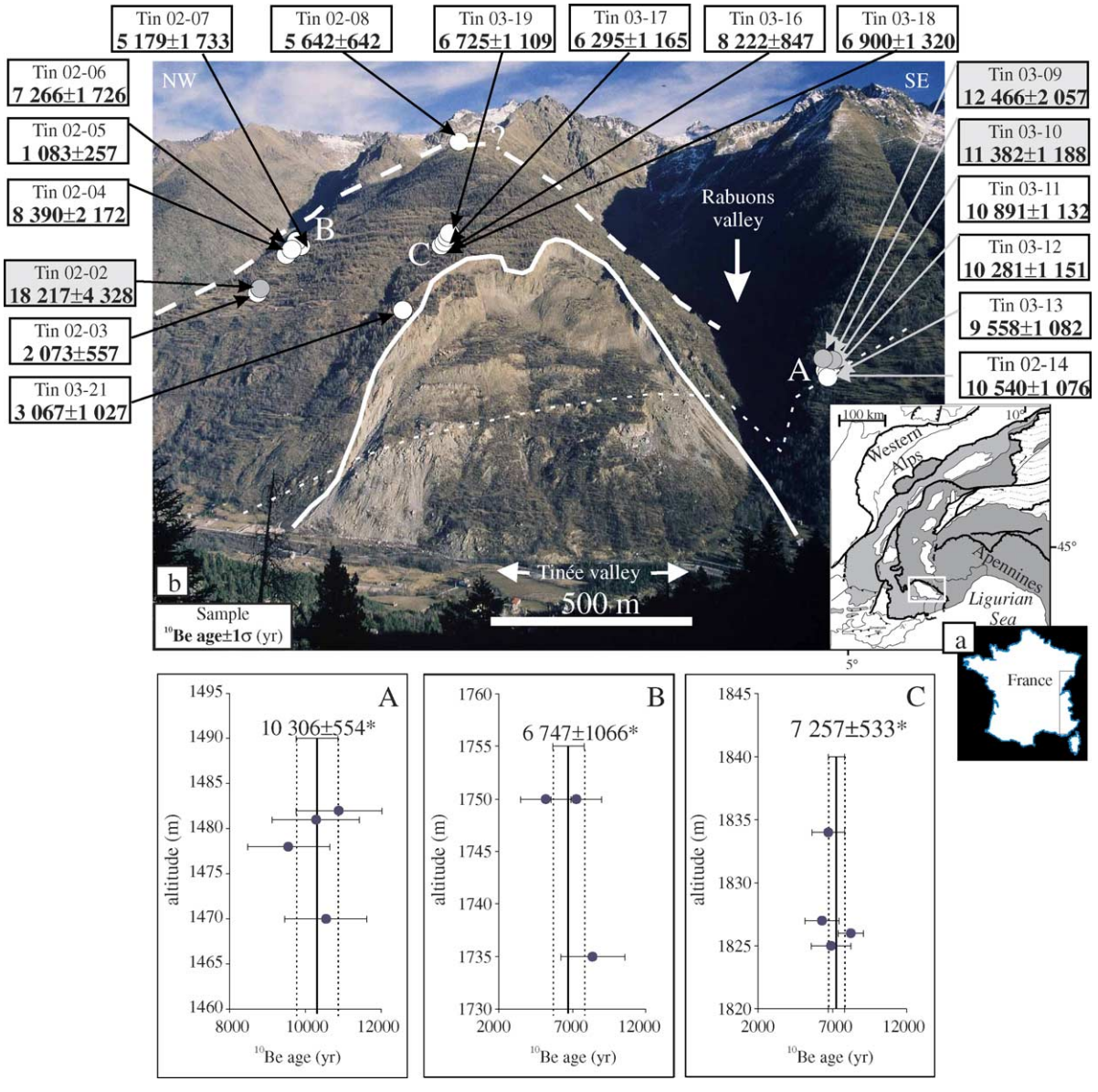

Fig. 1. (a) Location of the Argentera massif area (white rectangle) in the South of Western Alps, France. (b) Photo of the La Clapière landslide (located in the NW of the Argentera massif) with the location of analyzed samples. White circles correspond to samples coming from scarps, gray circles are samples coming from "stoss-and-lee" topography. *, weighted ages for sites A, B and C. The white line represents the active landslide area, the white dash line corresponds to the supposed limit of the destabilized area (historically "stable" area) and the white dot line is the shape of the main fault linking the Tinée and Rabuons valleys.

10; Table 1) from the glacial landform to date the glacier retreat and four samples from the scarp (Tin 03-11 to -14; Table 1) to date gravitational deformations.

Following methods described elsewhere [16], quartz was isolated and purified from samples and targets prepared for analyses of ^{10}Be. These analyses were undertaken at the Tandétron Accelerator Mass

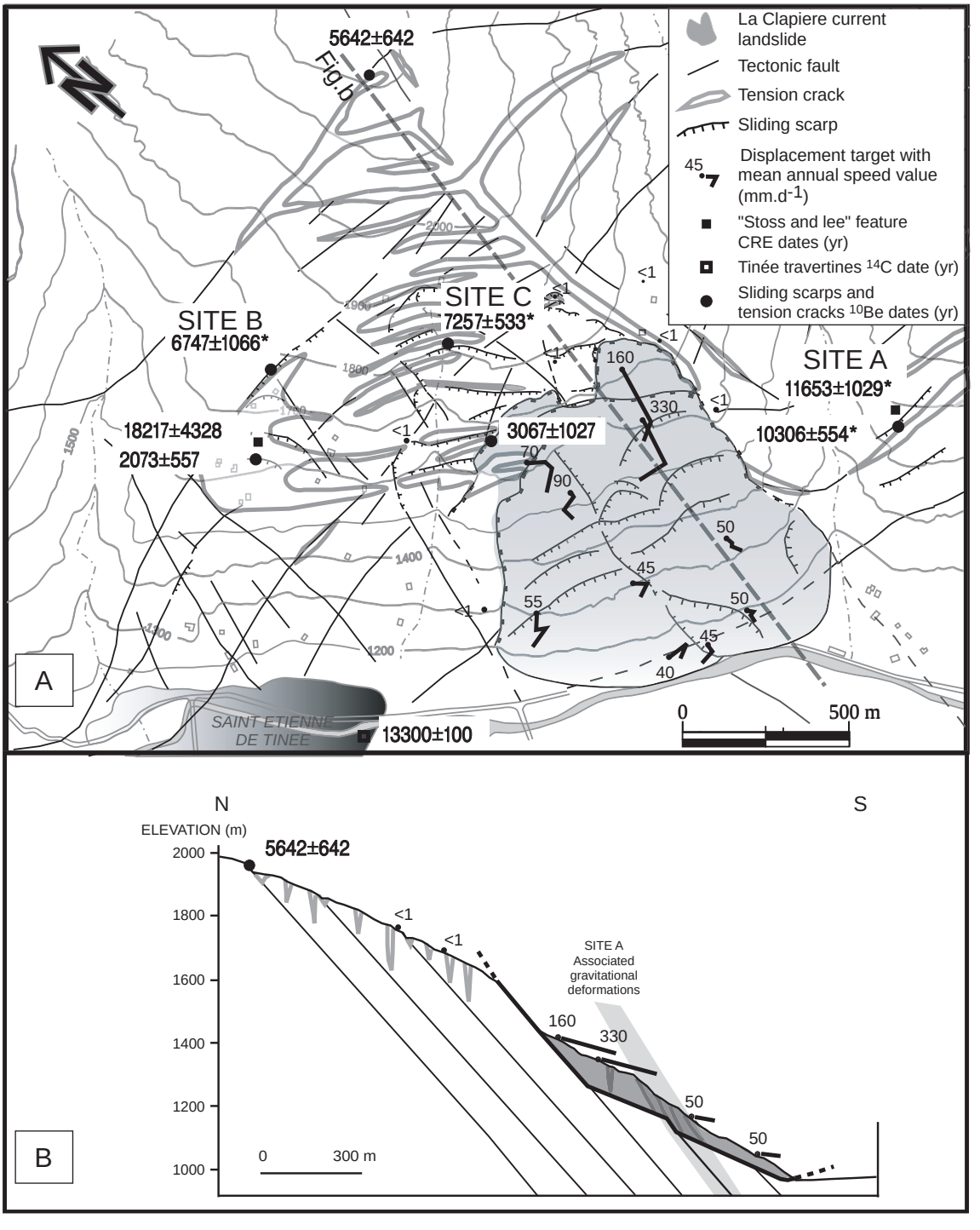
La Clapiere current landslide
Tectonic fault
Tension crack
Sliding scarp
Displacement target with mean annual speed value (mm.d-1)
"Stoss and lee" feature CRE dates (yr)
Tinée travertines 14C date (yr)
Sliding scarps and tension cracks 10Be dates (yr)
5642±642
Fig.b
SITE B
6747±1066*
SITE C
7257±533*
SITE A
11653±1029*
18217±4328
2073±557
3067±1027
10306±554*
13300±100
SAINT ETIENNE DE TINEE
A
0
500 m
N
S
ELEVATION (m)
SITE A
Associated gravitational deformations
B
0
300 m

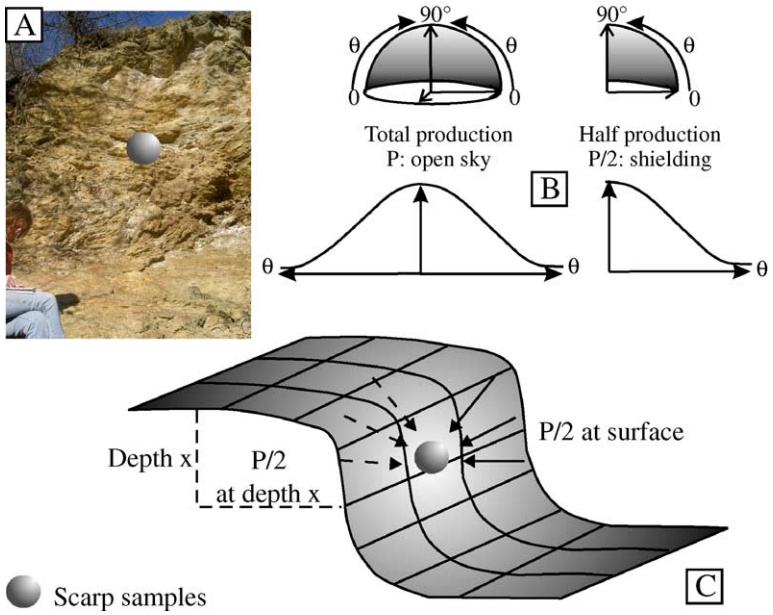

Fig. 3. (A) Photo illustrating the geometry of the bulk of scarps (several meters high) collected at different elevations for this study. (B) Diagrams showing the difference of ^{10}Be production according to the shielding (θ). When a sample is well exposed, just below an open sky, the ^{10}Be production is total. If a sample is located on a sub-vertical surface like on a scarp, this sample records the half production. (C) Sketch based on the scarps geometry illustrating the ^{10}Be total production obtained for a sample. Continuous arrows correspond to the ^{10}Be production accumulated by the sample directly on the scarp (vertical surface). Dotted arrows correspond to cosmic ray production after to have crossed the sampling depth (x) from the horizontal surface. This model was used to calculate the ^{10}Be ages (see text).

Spectrometer at Gif-sur-Yvette, France [17] using the National Institute of Standards and Technology (NIST) ^{10}Be standard (SRM 4325). Analytical uncertainties (reported as 1σ) are based on counting statistics, an additional conservative 3% uncertainty based on long-term measurements of standards, and a 50% uncertainty in the chemical and analytical blank correction.

Altitudinal and latitudinal variations in cosmogenic nuclide production rate are commonly modeled using empirical polynomials [18–20]. At the latitudes and altitudes of our studied region, these different models do not yield significantly different production rate corrections (less than 4%). Because it is located in the same latitudinal and altitudinal range as our study region and covers an equivalent expected time span, the calibrated production rate of the well dated Koefels landslide (21.8 ± 0.6 atom g^{-1} yr^{-1}) was used [21]. Koefels production rate covers the same time span as our study, and has independently been determined with calibrated ^{14}C. Then, it integrates any geomagnetic field variations (dipolar and multipolar variations); as a consequence, we did not correct our ages for these field effects. Production rates at the individual sampling sites were corrected for exact sampling latitude using the correction factors of Lal [18]; corrections of elevation were performed using the difference of air pressure from our site and Koefels (Standard Atmosphere Computations (http://aero.

Fig. 2. (A) Morpho-structural data represented on a topographical map underlying (i) the displacement rates (mm d^{-1}) in the active landslide and their directions, (ii) the tectonic pattern and scarps existing both in the active landslide and in the historically "stable" zone. "*" corresponds to uncertainty-weighted mean ages. (B) N–S cross-section from the top of the "stable" zone to the bottom of the active landslide with displacement rates recorded since the 1970s. This cross-section allows to locate the site A associated gravitational deformations crossing the Rabuons valley up to the bottom of the La Clapière landslide.

Table 1
Cosmogenic ^{10}Be analytical data

Sample	Location 44°15N	Altitude (m)	Distance from top of the scarp (cm)	Production rate (atom g^{-1} yr^{-1})[a]	[^{10}Be] (at/g)	[^{10}Be] error (atom g^{-1})	$T_{min} \pm 1\sigma$ (yr)
Scarps							
Site A							
Tin 03-11	Rabuons valley	1482	20	16.48	174,505	18,136	10,891 ± 1132
Tin 03-12	Rabuons valley	1481	80	16.48	120,993	13,542	10,281 ± 1151
Tin 03-13	Rabuons valley	1478	430	12.41	68,578	7760	9558 ± 1082
Tin 03-14	Rabuons valley	1470	1230	12.38	148,979	15,210	10,540 ± 1076
Site B							
Tin 02-05	Tinée side	1740	0	19.31	23,929	5686	1083 ± 257
Tin 02-04	Tinée side	1735	0	17.75	154,548	40,183	8390 ± 2172
Tin 02-06	Tinée side	1750	0	20.77	172,360	40,953	7266 ± 1726
Tin 02-07	Tinée side	1750	0	20.96	124,072	41,524	5179 ± 1733
Site C							
Tin 03-16	Tinée side	1826	70	19.46	118,518	12,207	8222 ± 847
Tin 03-17	Tinée side	1827	0	19.46	139,990	25,901	6295 ± 1165
Tin 03-18	Tinée side	1825	190	19.46	80,440	15,392	6900 ± 1320
Tin 03-19	Tinée side	1834	0	19.69	151,224	24,948	6725 ± 1109
Others							
Tin 02-08	Tinée side	2221	0	30.09	193,974	22,072	5642 ± 642
Tin 02-03	Tinée side	1610	0	18.08	42,870	11,530	2073 ± 557
Tin 03-21	Tinée side	1602	0	17.88	62,693	20,982	3067 ± 1027
Stoss-and-lee feature							
Tin 02-02	Tinée side	1615	0	18.15	376,744	89,516	18,217 ± 4328
Tin 03-09	Rabuons valley	1482	0	16.48	234,412	38,672	12,466 ± 2057
Tin 03-10	Rabuons valley	1482	0	16.48	214,075	22,350	11,382 ± 1188

[a] Production calculated following Lal [18], corrected from shielding [22] and based on production deduced from Kubik and Ivy-Ochs [21].

stanford.edu/StdAtm.html) were used). All production rate were normalized to eliminate the effects of shielding by local topography following the methods of Dunne et al. [22]. Local shielding factors range from 0 to 0.26.

Because these production rates are based on measurements calibrated against standards consistent with a value of 3.06×10^{-11} for the NIST standard [23,24], they were decreased by a factor of 0.875 for use with our measurements, which were calibrated against the NIST certified value of 2.68×10^{-11}. For comparison of exposure ages within a given landform or region, ages are reported in terms of "^{10}Be years" propagating experimental uncertainties for individual samples, but disregarding systematic uncertainties in production rates [25,26]. Comparison of these ages with absolute ages thus requires propagation of an additional 15% uncertainty for production rates.

To determine the scarp exposure ages the following equation was used:

$$C(x,t) = \frac{\frac{P_0}{2}.P_n}{\frac{\varepsilon}{\Lambda_n}+\lambda}.\left[1-\exp\left(-t.\left(\frac{\varepsilon}{\Lambda_{\mathrm{n}}}+\lambda\right)\right)\right] \times\left\{1+\exp\left(-\frac{x}{\Lambda_n}\right)\right\}+\frac{\frac{P_0}{2}.P_{\mu s}}{\frac{\varepsilon}{\Lambda_{\mu s}}+\lambda} .\left[1-\exp\left(-t.\left(\frac{\varepsilon}{\Lambda_{\mu s}}+\lambda\right)\right)\right] \times\left\{1+\exp\left(-\frac{x}{\Lambda_{\mu s}}\right)\right\}+\frac{\frac{P_0}{2_0}.P_{\mu f}}{\frac{\varepsilon}{\Lambda_{\mu f}}+\lambda}$$

$$\cdot\left[1-\exp\left(-t.\left(\frac{\varepsilon}{\Lambda_{\mu f}}+\lambda\right)\right)\right]$$

$$\times\left\{1+\exp\left(-\frac{x}{\Lambda_{\mu f}}\right)\right\}$$

where P_0 is the production rate; p_n, $p_{\mu s}$ and $p_{\mu f}$ refer to the neutron, slow and fast muons contributions, (these are 97.85%, 1.5% and 0.65%, respectively); Λ_n, $\Lambda_{\mu s}$ and $\Lambda_{\mu f}$ are the neutron, slow and fast muons attenuation lengths, which are 150, 1500 and 5300 g/cm^2 [27], respectively; λ is the radioactive decay constant, and ε is the erosion rate.

As described in Fig. 3 for each scarp sample, it has been assumed that ^{10}Be has been produced for one half of the total corrected production at depth x and for the second half at surface.

3. Results

Cosmic ray exposure ages of two "stoss-and-lee" feature samples located on the left bank of the Rabuons valley, close to the main feature linking the Tinée and Rabuons valleys, and at an elevation of 1482 m, yield non-significantly different ^{10}Be ages of 12.5 ± 2.0 ^{10}Be ka and 11.4 ± 1.2 ^{10}Be ka (Table 1; Fig. 1b). These ages, which constrain the timing of the deglaciation in the Rabuons valley at that elevation, are indistinguishable from the ^{10}Be ages obtained along the nearby gravitational scarp (Site A) whose uncertainty-weighted mean age is 10.3 ± 0.5 ^{10}Be ka (Table 1; Fig. 1b).

Consistently, the CRE age of a "stoss-and-lee" topography sampled at an elevation of 1,615 m on the La Clapière slope constrains the timing of the deglaciation in the Tinée valley at that elevation at 18.2 ± 4.3 ^{10}Be ka (Table 1; Fig. 1b). Two distinct gravitational scarps (Tin 02-03, Tin 03-21) sampled at an elevation similar to that of the La Clapière "stoss-and-lee" feature yield non-significantly different CRE ages of 2.1 ± 0.6 ^{10}Be ka and 3.1 ± 1.0 ^{10}Be ka, respectively (Table 1; Fig. 1b).

Excluding an apparent outlier (Tin 02-05), the CRE ages range for samples from a gravitational scarp located at an altitude of ~ 1750 m (Site B) is 5.2 ± 1.7 to 8.4 ± 2.2 ^{10}Be ka, yielding an uncertainty-weighted mean age of 6.7 ± 1.1 ^{10}Be ka (Table 1; Fig. 1b). The younger CRE age of sample Tin 02-05 (Table 1) may be interpreted as the result of burial below ~ 100 cm of soil most of the time preceding the sampling.

Samples from another gravitational scarp located slightly upward at an altitude of ~ 1825 m (Site C) yield CRE ages ranging from 6.3 ± 1.2 to 8.2 ± 0.8 ^{10}Be ka (Table 1; Fig. 1b). The implied uncertainty-weighted mean age of 7.2 ± 0.5 ^{10}Be ka is indistinguishable from that deduced for Site B (Fig. 1b).

Sample Tin 02-08 collected in a part of the La Clapière slope previously considered as not affected by gravitational destabilization yields a CRE age of 5.6 ± 0.6 ^{10}Be ka similar to those of sites B and C (Table 1; Fig. 1b). This sample thus allows extending the limit of the gravitationally destabilized area.

4. Discussion and conclusion

Our results on glacial landforms allow reinforcing local glacial chronology deduced from geomorphological features and those on gravitational features provide constrains on the chronology of the successive destabilizations leading to the observed large active landslide.

In the lateral valley of Mollières (SW of the Argentera massif), high altitude moraines emplaced during the Dryas II glacial pulsation [28], whose median age is ~ 14,500 cal. BP in the Southern Alps [29], lead to a line of permanent snows, established following the Hoefer's method [30], ranging from 1800 to 2100 m at that time period. In the main Tinée valley, the front of the Würmian glacier corresponding to the last glacial maximum was slightly downstream of Saint-Sauveur (SW from the valley of Mollières). At the confluence with the valley of Mollières, the surface of this glacier reached around 1000 m in altitude [28]. The glacial maximum having been recently dated at $21{,}580 \pm 960$ yr cal. BP in the Southern Alps [31], these geomorphological constraints imply that during the time interval 21,580–14,500 cal. BP the glacier retreats at a speed ranging from 0.093 m yr^{-1} to 0.195 m yr^{-1}. Within uncertainties, this is consistent with the ^{10}Be CRE age of 18.2 ± 4.3 ^{10}Be ka obtained at an altitude of ~ 1600 m, just above Saint-Etienne de Tinée. In addition, a ^{14}C age of 13.3 ± 0.1 ka obtained for this study, from a travertine located at 1100 m within the Tinée valley (Fig. 2A), confirms that it was

totally deglaciated at that time. By contrast, CRE dating of "stoss-and-lee" feature from the Rabuons lateral valley leads to propose that it is totally deglaciated since only less than ~ 10 ka ago.

The gravitational destabilization dated at 10.3 ± 0.5 ^{10}Be ka on the left bank of the Rabuons valley (Site A) moving the glacial landform dated at 11.6 ± 1.0 ^{10}Be ka (Fig. 2A), thus appears most likely linked to the slope decompression resulting from this late deglaciation, as previously proposed by Gunzburger [32] at the local scale, and by others [33,34] at the Alps scale. Nevertheless, the Tinée valley was totally deglaciated at about 13 ^{10}Be ka, and none scarp was dated in this slope at about 12,000–13 000 yr. So even if we observe a local slope decompression which would trigger the initial gravitational destabilization since the dated scarp extends to the bottom of the Tinée valley under the present landslide (Figs. 1b and 2A,B), the Tinée valley glacier retreat does not seem to be the trigger of gravitational destabilizations of the La Clapiere slope which start more than 3000 yr after.

The indistinguishable CRE ages obtained from sites B and C gravitational scarps strongly suggest a second gravitational destabilization phase at 7.1 ± 0.5 ^{10}Be ka (Table 1), which is during the last Holocene "climatic optimum" characterized by a forest cover development (Fig. 4). However, it is evidently impossible to argue that this second gravitational destabilization is only linked to this global climatic change. It may as well result either from a catastrophic event, such as an earthquake, on the Tinée valley scale, or from post-glacial isostatic rebound on the alpine arc scale. Similar considerations can be made

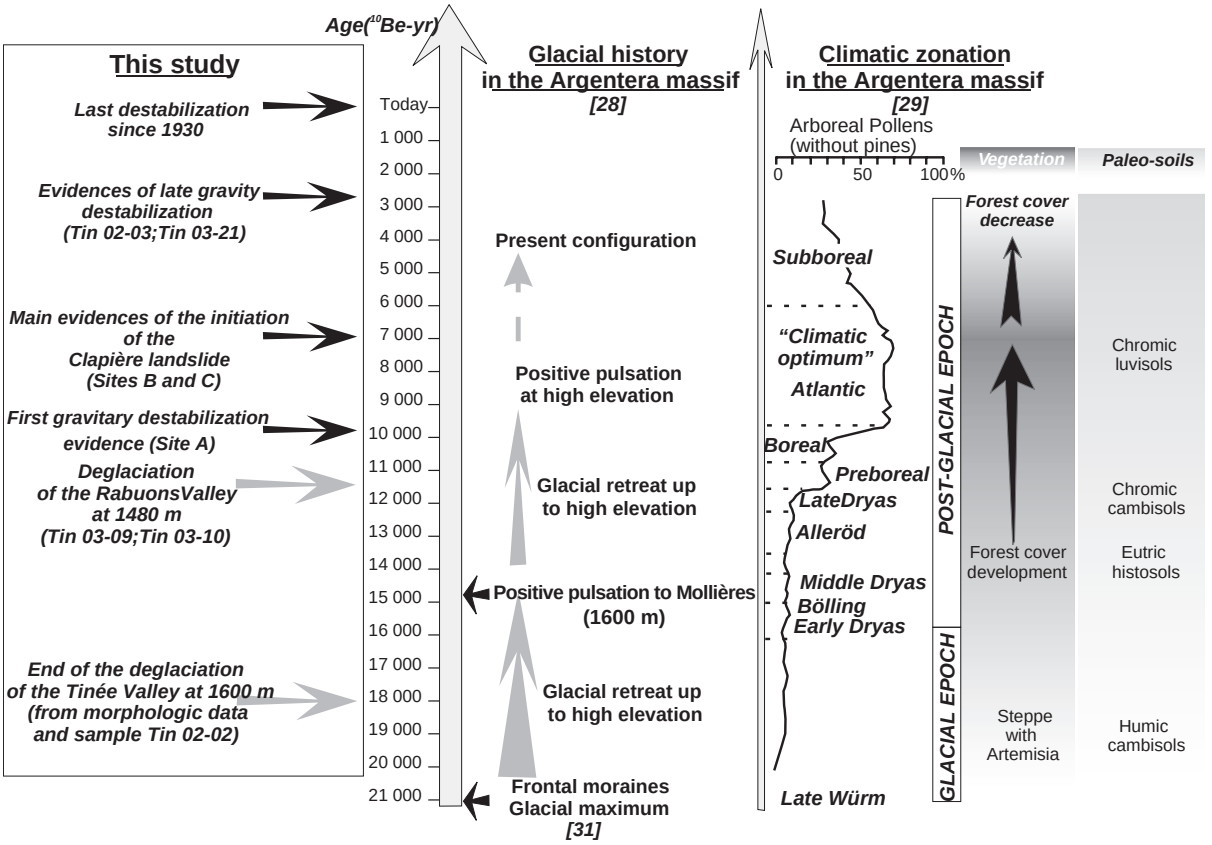

Fig. 4. Synthesis of climatic data since the last glacial maximum in the Argentera massif compared to the glacial dynamic in the Tinée valley and the first destabilizations of the Clapière Landslide.

for the destabilization phase evidenced at 2.3 ± 0.5 ^{10}Be ka (Table 1, Tin 02-03 and 03-21), except that there is no characterized global climatic event during that time period.

The demonstrated ability using in situ produced cosmogenic ^{10}Be to establish the chronology of the gravitational destabilizations leading to present major active landslides allows investigating the various triggering processes on a large timescale. This study clearly shows that the present La Clapière landslide does not only and simply result from the last deglaciation decompression. Other destabilizations triggered either by humidity during the climatic optimum, or by post-glacial isostatic rebound, or by local effects, or by a combination of some of these parameters, occurred [35]. To decipher between these scenarios, similar studies on other landslides inside the alpine arc will be necessary.

Finally, this first study also shows that same gravitational failure surfaces within a slope undergo several activity and no-activity periods. Part of the 2.3 ± 0.5 ^{10}Be ka old scarps is the actual active La Clapière scarp (which is about 100 yr old; [12]). This is in agreement with other works [36] that show that the structural control of pre-existing brittle structures is one of the most important driving factors of the evolution of large slope instabilities. This means that to fully understand the processes leading to current major landslides and, thus, to assess the mass wasting, large space and time scales have to be considered. For example, at least in the Alps, the last 20,000 yr and the entire slope from the valley to the crests have to be considered and not only the few years of historical activity of an active landslide.

Acknowledgement

We wish to thank G. Aumaitre and M. Arnold, the engineers of the Tandetron accelerator mass spectrometry (ASM) facility at Gif-sur-Yvette (France) who help us to obtain our data. Geosciences Azur contribution no. 743.

References

[1] B. Finlayson, I. Statham, Hillslope Analysis, Heineman, London, 1980, 230 pp.

[2] M. Julian, E. Anthony, Aspects of landslide activity in the Mercantour massif and the French Riviera, southeastern France, Geomorphology 15 (1996) 175–289.

[3] F. Noverraz, C. Bonnard, H. Dupraz, L. Huguenin, Grands glissements de versant et climat, Rapport final du PNRN VERSINCLIM, No. ISBN 3 7281 2612 8, VDF Ed., Hochschulverlag AG an der ETH Zürich, ETH Zentrum, CH-8092 Zürich, (1998) 314 pp.

[4] J.F. Shroder, Mass movement in the Himalaya: an introduction, Geomorphology 26 (1998) 9–11.

[5] F. Agliardi, G. Crosta, A. Zanchi, Structural constraints on deep-seated slope deformation kinematics, Engineering Geology 59 (2001) 83–102.

[6] A. Faure-Muret, Etudes géologiques sur le Massif de l'Argentera-Mercantour et sur ses enveloppes sédimentaires, Mémoire de la Carte géologique de France, 336 pp.

[7] S. Bogdanoff, Evolution de la partie occidentale du massif de l'Argentera. Place dans l'arc alpin, Géologie de la France 4 (1986) 433–453.

[8] R. Malaroda, F. Carraro, G.V. Dal Piaz, B. Franceschetti, C. Sturani, E. Zanella, Carta geologica del Massiccio dell'Argentera alla scala 1/50000 Note illustrative, Memorie della Societa Geologica Italiana 9 (1970) 557–663.

[9] F. Bigot-Cormier, G. Poupeau, M. Sosson, Dénudations différentielles du massif cristallin externe alpin de l'Argentera (Sud-Est de la France) révélées par thermochronologie traces de fission (apatites, zircons), Compte Rendu de l'Académie des Sciences de Paris 330 (2000) 363–370.

[10] F. Bigot-Cormier, M. Sosson, G. Poupeau, J.-F. Stéphan, E. Labrin, The denudation history of the Argentera Alpine External Crystalline Massif (France–Italy): an overview from the analysis of fission tracks in apatites and zircons, Tectonophysics (in press).

[11] F. Cappa, Y. Guglielmi, V.M. Soukatchoff, J. Mudry, C. Bertrand, A. Charmoille, Hydromechanical modeling of a large moving rock slope inferred from slope levelling coupled to spring long term hydrochemical monitoring: example of La Clapière landslide (Southern Alps, France), Journal of Hydrology 291 (2004) 67–90.

[12] J.P. Follacci, Seize ans de surveillance du glissement de la Clapière (Alpes-Maritimes), Bulletin des Laboratoires des Ponts et Chaussées 220 (1999) 35–51.

[13] Guglielmi, C. Bertrand, F. Compagon, J.P. Follacci, J. Mudry, Acquisition of water chemistry in a mobile fissured basement massif: its role in the hydrogeological knowledge of the La Clapiere landslide (Mercantour massif, Southern Alps, France), Journal of Hydrology 229 (2000) 138–148.

[14] Y. Gunzburger, B. Laumonier, Origine tectonique du pli supportant le glissement de terrain de la Clapière (NW du massif de l'Argentera-Mercantour, Alpes du Sud, France) d'après l'analyse de la fracturation, Compte Rendu de l'Académie des Sciences de Paris 334 (2002) 415–422.

[15] J.C. Gosse, F.M. Philips, Terrestrial in situ cosmogenic nuclides: theory and application, Quaternary Scientific Revue 20 (2001) 1475–1560.

[16] E.T. Brown, J.M. Edmond, G.M. Raisbeck, F. Yiou, M.D. Kurz, E.J. Brook, Examination of surface exposure ages of

moraines in Arena Valley, Antarctica, using in situ produced ^{10}Be and ^{26}Al, Geochimica and Cosmochimica Acta 55 (1991) 2269–2283.

[17] G.M. Raisbeck, F. Yiou, D.L. Bourlès, E. Brown, D. Deboffle, P. Jouhanneau, J. Lestringuez, Z.Q. Zhou, The AMS facility at Gif-sur-Yvette, progress, perturbations and projects, Nuclear Instruments and Methods in Physic Research, B 92 (1994) 43–46.

[18] D. Lal, Cosmic ray labelling of erosion surfaces: in situ nuclide production rates and erosion models, Earth and Planetary Science Letters 104 (1991) 424–439.

[19] T.J. Dunai, Scaling factors for production rates of in situ produced cosmogenic nuclides: a critical reevaluation, Earth and Planetary Science Letters 176 (2000) 157–169.

[20] J.O. Stone, Air pressure and cosmogenic isotope production, Journal of Geophysical Research 105 (2000) 23753–23759.

[21] P.W. Kubik, S. Ivy-Ochs, A re-evaluation of the 0–10 ka ^{10}Be production rate for exposure dating obtained from the Köfels (Austria) landslide, Nuclear Instruments and Methods in Physics Research, B 223–224 (2004) 618–622.

[22] A. Dunne, D. Elmore, P. Muzikar, Scaling of cosmogenic nuclide production rates for geometric shielding at depth on sloped surfaces, Geomorphology 27 (1999) 3–11.

[23] R. Middleton, L. Brown, B. Dezfouly-Arjomandy, J. Klein, On ^{10}Be standards and the half-life of ^{10}Be, Nuclear Instruments and Methods in Physics Research, B 82 (1993) 399–403.

[24] E.T. Brown, T.W. Trull, P. Jean-Baptiste, G.M. Raisbeck, D.L. Bourlès, F. Yiou, B. Marty, Determination of cosmogenic production rates of ^{10}Be, ^{3}He, and ^{3}H in water, Nuclear Instruments and Methods in Physics Research, B 172 (2000) 876–886.

[25] J.C. Gosse, J. Klein, E.B. Evenson, B. Lawn, R. Middleton, Beryllium-10 dating of the duration and retreat of the last Pinedale glacial sequence, Science 268 (1995) 1329–1333.

[26] E.T. Brown, D.L. Bourlès, B. Burchfield, Q. Deng, J. Li, P. Molnar, G.M. Raisbeck, F. Yiou, Estimation of slip rates in the southern Tien Shan using cosmic ray exposure dates of abandoned alluvial fans, Geological Society of America Bulletin 110 (1998) 377–386.

[27] R. Braucher, E.T. Brown, D.L. Bourlès, F. Colin, In situ-produced ^{10}Be measurements at great depths: implications for production rates by fast muons, Earth and Planetary Science Letters 211 (2003) 251–258.

[28] M. Julian, Les Alpes franco-Italiennes, Etude Géomorphologique, Thesis, Université d'Aix-Marseille (France), 1980, 836 pp.

[29] J.L. Beaulieu, Contribution pollenanalytique à l'histoire tardiglaciaire et holocène de la végétation des Alpes méridionales françaises, Thesis, Université d'Aix-Marseille (France), 1977, 391 pp.

[30] G. Schweizer, Le Tardiglaciaire et le niveau des neiges permanentes dans les hautes montagnes des Alpes-Maritimes, Méditerranée 9-l (1968) 23–40.

[31] M. Jorda, T. Rosique, J. Evin, Données nouvelles sur l'âge du dernier maximum glaciaire dans les Alpes méridionales françaises, Compte Rendu de l'Académie des Sciences de Paris 331 (2000) 187–193.

[32] Y. Gunzburger, Apports de l'analyse de la fracturation et de la modélisation numérique à l'étude du versant instable de la Clapière, Thesis, INPL, Nancy (France), 2001, 81 pp.

[33] G. Barla, E. Chiriotti, Insights into the behaviour of the large deep seated gravitational slope deformation of Rosone, in the Piemont Region (Italy), Felsbau 13 (1995) 6.

[34] G. Crosta, Landslide, spreading, deep seated gravitational deformation: analysis, examples problems and proposals, Geografia Fisica Dinamica Quaternaria 19 (1996) 297–313.

[35] J.B. Thornes, I. Alcantara-Ayala, Modelling mass failure in a Mediterranean mountain environment: climatic, geological, topographical and erosional controls, Geomorphology 24 (1998) 87–100.

[36] G. Crosta, A. Zanchi, Deep seated slope deformations. Huge, extraordinary, enigmatic phenomena, in: E. BromheadProceedings of the 8th International Symposium on Landslides, Cardiff, June 2000.